Available online at www.sciencedirect.com

SciVerse ScienceDirect

Ceramics International 38 (2012) 1347–1352

CERAMICS INTERNATIONAL

www.elsevier.com/locate/ceramint

Nanoindentation behaviour of nano $BiFeO_3$

Pintu Sen [a], Arjun Dey [b,1], Anoop K. Mukhopadhyay [b,*], S.K. Bandyopadhyay [a], A.K. Himanshu [a]

[a] *Variable Energy Cyclotron Centre, 1/AF, Bidhan Nagar, Kolkata 700064, India*

[b] *Mechanical Property Evaluation Section, CSIR-Central Glass and Ceramic Research Institute, Jadavpur, Kolkata 700064, India*

Received 30 July 2011; received in revised form 3 September 2011; accepted 3 September 2011

Available online 10 September 2011

Abstract

Bismuth ferrite ($BiFeO_3$) is a unique magnetoelectric multiferroic that exhibits the coexistence of ferroelectricity and antiferromagnetism at room temperature. This unique combination of properties has pumped a huge surge in current research on $BiFeO_3$ as a future material for very important technological applications such as magnetic detectors and as an active layer in magnetoelectric memories. For such applications involving miniaturized components and devices, it is essentially important to have an idea of the mechanical integrity of the system at the scale of the microstructure. In spite of the wealth of the literature, however, the attempt to evaluate the mechanical integrity of nano $BiFeO_3$ at a scale comparable with the local microstructural length scale was almost non-existent. Here we report, possibly for the first time the nanoindentation behaviour of a sol–gel process derived nano $BiFeO_3$ having particle size of 5–25 nm. The nanoindentation studies were conducted at 100–1000 μN loads on a green pellet annealed at a low temperature of only 300 °C to avoid particle coarsening. The results showed interesting dependence of nanohardness and Young's modulus on the nanoindentation load which could be explained in terms of elastic recovery and plastic deformation energy concepts.

Keywords: Nano $BiFeO_3$; Multiferroic; Nanoparticle; Nanoindentation

1. Introduction

Bismuth ferrite ($BiFeO_3$) is a well known magnetoelectric multiferroic (MM) material [1,2]. MM materials are being coined as an '*accidental beauty of nature*'. The beauty of these materials is that in them the ferroelectricity and magnetism coexist in a coupled fashion. Currently there is a huge research interest in these MM materials in general and in bismuth ferrite in particular. The possible applications of these materials include both magnetic detectors and multi-state memory devices. The fundamental research interest in such materials also stem from the fact that the complex yet interesting physics behind the fundamental mechanisms for magnetoelectric coupling is still far from well understood. Bismuth ferrite (BFO) stands out in the '*genre*' of MM materials which are being most actively researched upon these days simply because of the fact that it is the only known *room temperature* MM material in which both ferroelectricity and antiferromagnetism coexist [1,2].

It exhibits huge remnant polarization ($\sim$100 μC cm^{-2}) in both single crystal [3,4] and thin film form [5,6]. It also displays very attractive feature of the coupling between the directions of the ferroelectric polarization and the sublattice magnetization [7]. These unique features have inspired the consideration of BFO as the active layer in magnetoelectric memories based on exchange bias and also as a possible active material in the next generation of lead-free ferroelectric materials.

BFO has a superimposed incommensurate *G-type cycloid spin structure* with a periodicity of 62 nm along the $[1\,1\,0]_h$ direction in its rhombohedral structure [1,2,6]. At room temperature it possesses a rhombohedrically distorted perovskite structure (space group *R*3*c*). The unique beauty is that this structure is both ferroelectric (with polarization along the <1 1 1> directions and antiferromagnetic [8]). It has been reported that at a temperature of $\sim$827 °C BFO shows a transition from rhombohedral to orthorhombic [6] or monoclinic [7]

* Corresponding author. Present address: Central Glass and Ceramic Research Institute, 196, Raja S.C. Mullick Road, Kolkata 32, India. Tel.: +91 33 2473 3469/76/77/96; fax: +91 33 2473 0957.

E-mail address: anoopmukherjee@cgcri.res.in (A.K. Mukhopadhyay).

[1] Presently the author is associated with the Thermal System Group, ISRO Satellite Centre (ISAC), Indian Space Research Organisation, Dept. of Space, Govt. of India, Bangalore, India.

0272-8842/$36.00
doi:10.1016/j.ceramint.2011.09.011

symmetry. However, at a temperature of ~927 °C it becomes cubic [6,7]. It displays both ferroelectricity with a relatively high Curie temperature (T_C = 820–850 °C) and antiferromagnetic properties below the Neel temperature (T_N = 350–380 °C) [1,2,6]. The antiferromagnetic symmetry is itself very attractive to researchers because it exhibits a long period (62 nm) cycloidal helix of spins which is not commensurate with the lattice periodicity [8,9].

The recent major challenge has been to synthesize this material in nanostructured form i.e. to prepare nano BFO (NBFO) to exploit better the functionalities of this MM material in various dimensions. Another remarkable ordering to be achieved is in the line of '*ferroelasticity*', particularly in nanomaterials. For instance, ferroelastic ordering has been observed in La based perovskites [10,11] through studies on mechanical hysteresis due to plastic deformation. Similarly, measurement of Young's modulus specifically at low temperatures between 120 and 290 K on bulk ceramic BFO bars in three-point bending configuration showed [12] stiffening of ≈10% upon cooling accompanied by a simultaneous peak in dissipation (tan δ) which was suggested to be an indication of transition from a dynamically relaxed system above 230 K to an unrelaxed state below this temperature. Recent phenomenological analysis [13] for rhombohedral BFO film reveals that both the depolarizing energy and the elastic energy are indispensable for the equilibrium domain structures. It was noted further that with the increase in the asymmetrical electrostatic boundary on the film surfaces, the dominant domain scaling mechanism changes from electrostatic-dependent domain structure to elastic-dependent one. Very recent report [14] on in situ neutron diffraction studies during the application of uniaxial compressive stress on polycrystalline, large grain, mixed phase $[(1-x)(Bi_{1-y}La_y)FeO_3$–$xPbTiO_3]$ (BF–PT) ceramics suggest that that the achievable strain in BF–PT is largely generated by straining of the rhombohedral phase. Clearly the amount of studies on mechanical behaviour of BFO or its composites are still far from significant. As a matter of fact, to the best of our knowledge there is no report on nanomechanical properties evaluation of NBFO. In the present communication, we report the systematic nanoindentation study at ultra low loads on NBFO material which has not been reported so far.

2. Materials and methods

The nano $BiFeO_3$ (NBFO) samples were prepared by sol–gel technique starting with the nitrates of the respective elements. Equimolar $Bi(NO_3)_3{\cdot}5H_2O$ and $Fe(NO_3)_3{\cdot}9H_2O$ were added successively into requisite amount of concentrated HNO_3 acid (65–68%). After the addition of tartaric acid (2–4 M), the solution was heated under stirring on a hot plate (~250 °C) until all the liquids evaporated out from the solution. Finally, the powder was pelletised at a pressure of 600–800 MPa. The green pellets were further annealed at a low temperature of only 300 °C to avoid grain coarsening. These NBFO samples were used for carrying out the experiment of nanoindentation to explore the mechanical properties at the scale of the local microstructure.

Phase identification and morphological characterizations of the NBFO samples were carried using an X-ray diffractometer (XRD: Philips PW 1710) with CuK_α (λ = 1.5406 Å) radiation and a transmission electron microscope (TEM: FEI model Tecnai G2 20S with 200 kV accelerating voltage and resolution of 0.2 nm). Prior to nanoindentation study, the NBFO pellet samples were subsequently polished with 0.25 μm diamond paste (Metadi II, Buehler, USA) and 0.04 μm silica suspension using a standard polishing machine (LaboPol-5, Struers, USA).

The nanoindentation experiments were conducted with a nanoindenter (TriboIndenter Ubi 700, Hysitron Inc., Minneapolis, USA). It had a load resolution of 1 nN along z-axis. The depth resolution was 0.04 nm along z-axis. The thermal drift was <0.05 nm s^{-1}. All the nanoindentation experiments whose results are reported in the present work were conducted at room temperature (~30 °C) and ~70% relative humidity. The machine provided a surface topography of constant contact force in scanning probe microscopy (SPM) mode and a load versus depth of penetration plot in nanoindentation mode using a tetrahedral diamond Berkovich tip of ~150 nm tip radius and semi-apex angle ~65.3°. The sample was mounted on a motorized table that allowed for a movement in the plane normal to the axial motion of the tip. The transducer that measured both load and depth consisted of a three-plate capacitor. It had the same tetrahedral diamond Berkovich tip of ~150 nm tip radius as mentioned above, attached to its central plate. The instrument was calibrated before each and every experiment by performing indents of increasing depth in a standard fused quartz sample provided by the supplier of the machine. The standard fused quartz sample had a known nanohardness of 9.25 ± 0.93 GPa and a reduced Young's modulus (E_r) of 69.6 ± 3.48 GPa. The diamond tip had a Poisson's ratio of 0.07 and Young's modulus of 1140 GPa [15]. The nanohardness and Young's modulus data of the present NBFO were calculated using the method of Oliver and Pharr [16]. In the present experiments, three different loads e.g. 100, 500 and 1000 μN were employed. At least 16 nanoindents (i.e. 4 × 4 array) were made at each of the five randomly chosen different locations of the sample. Thus, each reported value of nanohardness was an average of at least 80 or more individual data points.

3. Results and discussions

Fig. 1 shows the typical XRD pattern of the nano $BiFeO_3$ powder (JCPDS 71-2494) with small amount of Bi_2O_3 phase, as the synthesis was carried out at low temperature to achieve the particle of desired dimension. The TEM picture of synthesized $BiFeO_3$ nanoparticles (Fig. 2) confirmed that the sizes of the particles were in the range of 5–25 nm.

For the NBFO sample the typical load–depth (P–h) plots for nanoindentations made with a Berkovich indenter at three different loads (e.g. 100, 500 and 1000 μN) are shown in Fig. 3. The residual depth was much higher e.g. about 42 nm at higher indentation load (e.g. 1000 μN) than that (8 nm) at lower load

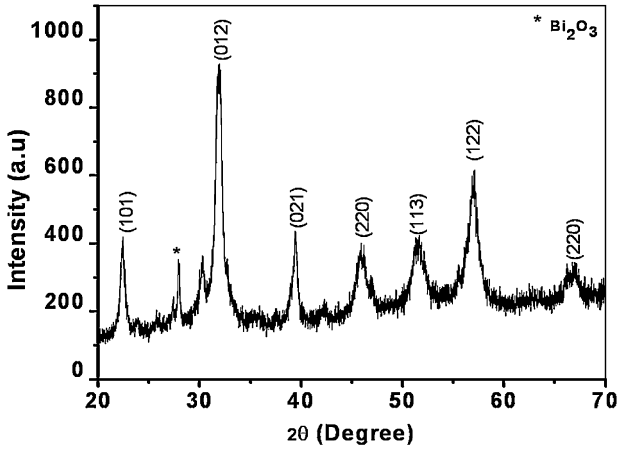

Fig. 1. XRD trace of nano $BiFeO_3$ (NBFO) powder.

e.g. 100 μN. Further, at higher load (e.g. 1000 μN) a larger area was encompassed by the *P–h* plot implying dissipation of higher amount of energy as compared to those involved at lower loads (e.g. 100 μN). The ratio of final depth of penetration (h_f) and maximum depth of penetration (h_m) was in the range of 0.37–0.43. The value of this ratio (h_f/h_m) should lie below 0.7 to obtain reliable results from the Oliver–Pharr model [16]. Thus, the range of values of h_f/h_m (e.g. 0.37–0.43) also justified the applicability of the Oliver–Pharr model to analyze the nanoindentation data of the present NBFO sample. Typical in situ SPM images of the impression of Berkovich indentation array at 500 and 1000 μN load on the NBFO sample are shown in Fig. 4a and b, respectively. There was no visible damage in the nanoindent impressions. However, the area of the impression was a little larger (e.g. $\sim 360.45 \times 10^3$ nm^2) at higher load e.g. 1000 μN load in comparison to that (e.g. $\sim 129.21 \times 10^3$ nm^2) at lower load e.g. 500 μN.

The indentation process is generally elastoplastic and forms a contact induced plastic deformation zone [17]. Since the measurement is on an extremely small area and the depth is low, generally a high hardness comparable with bulk samples is obtained e.g. as for thin films [18,19].

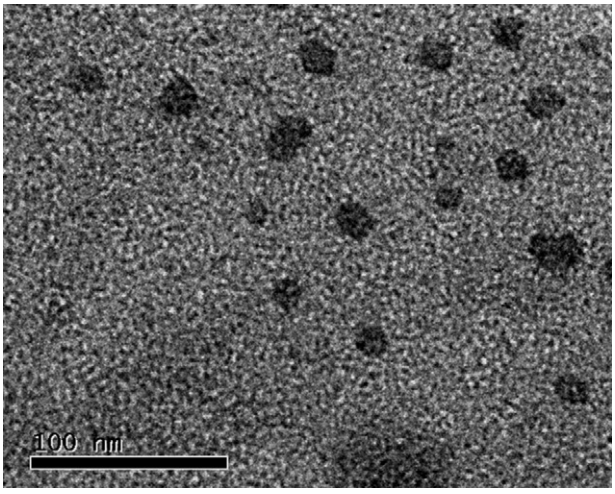

Fig. 2. TEM photomicrograph of nano $BiFeO_3$ (NBFO) powder.

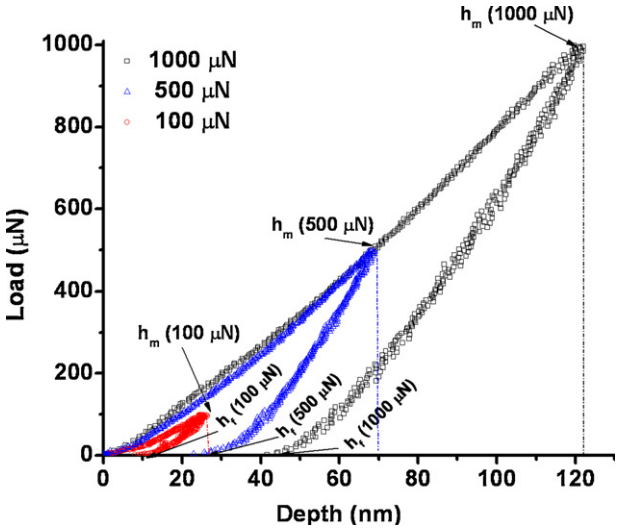

Fig. 3. Load–depth (*P–h*) plots for nanoindentations with a constant load of 100, 500 and 1000 μN on the green NBFO pellet.

Variations of data on nanohardness and Young's modulus as a function of indentation load (*P*) are shown in Fig. 5a and b, respectively. At a low load of 100 μN, the nano $BiFeO_3$ showed nanohardness (*H*) value ~3.8 GPa at a depth of ~8 nm which dropped to ~2.8 GPa at a depth of ~42 nm for a higher load of 1000 μN (Fig. 5a). The corresponding Young's modulus (*E*) values were ~51 GPa and ~26 GPa (Fig. 5b) at 100 and 1000 μN loads, respectively. Thus, the rate of change of the Young's modulus with load (*dE*/*dP*) was about 0.50 GPa μN^{-1}. Similarly, the rate of change of the nanohardness with load (*dH*/*dP*) was about 0.26 GPa μN^{-1}. The decrease in hardness with increasing load is the manifestation of indentation size effect and can be explained by the Nix and Gao model in terms of statistically stored and geometrically necessary dislocations [20]. Large strain gradients inherent in small indentations cause enhanced hardness.

In general, higher density and fine grained microstructure exhibits higher hardness and Young's modulus as is evident, for instance; from the comparison of data for hot isostatically pressed (HIPed) and normally sintered lead zirconium titanate (PZT) samples [21]. Nanomaterials can be considered to have minimum grain size and hence are expected to have high value of hardness and Young's modulus. Of course, in nanomaterials the presence of porosity causes indentation a bit difficult as evident from the in situ SPM images (Fig. 4). Typically green ceramics are about 60% of theoretical density. So, they have a residual porosity of about 40%. However, it should be mentioned in this connection that the residual porosity in the present NBFO sample was really small at about only 15% as found from the image analysis of the SPM images (Fig. 4). The reason for such small porosity was (a) very good packing density achievement due to the favourable shape (Fig. 2) of the initial particles obtained from the sol–gel process and (b) the very small average size of about 15 nm (e.g. range 5–25 nm) for the initial NBFO particles (Fig. 2) which helped attaining the high packing density. The porosity dependence of hardness is well known to originate from the change in solid load bearing

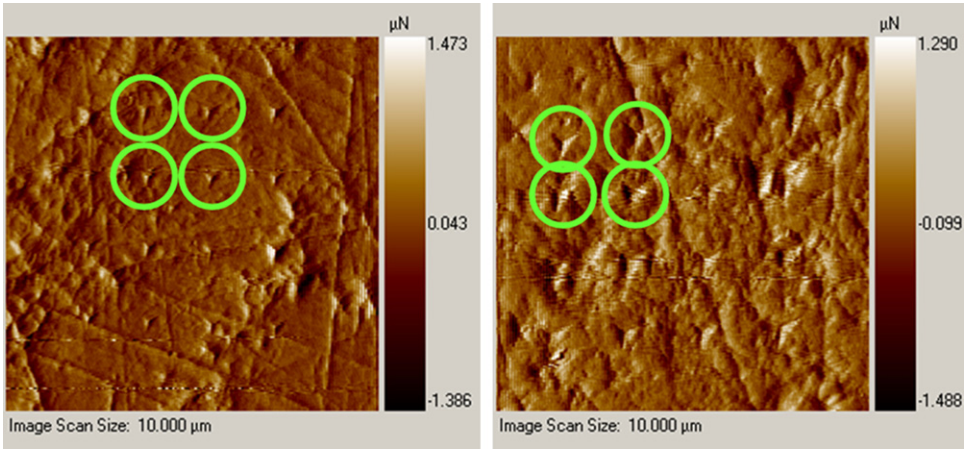

Fig. 4. In situ SPM photomicrographs (image scan size: 10 μm × 10 μm) of the green NBFO pellet showing the placement of the (a) 500 μN and (a) 1000 μN Berkovich nanoindentation array (green circles indicate the typical impression of the indents). (For interpretation of the references to color in this figure caption, the reader is referred to the web version of the article.)

area [22,23]. In other words the higher the porosity, the smaller the solid load bearing contact area, the lower the hardness and vice versa. Out of the empirically proposed exponential, linear, power and quadratic relationships between volume fraction open porosity P and measured hardness H [24–26]; the exponential porosity–hardness relationship was recently found to describe the experimentally found effect of porosity on nanohardness of brittle porous (e.g. $P = 11$–20%) ceramic coatings the best [27]. Taking the cue from there if an empirical relationship of $H = H_0$ Exp $(-bP)$ is assumed in the present work, then; taking the value of b as 4.5 [26], using our experimentally measured values of nanohardness, $H = 3.8$ and volume fraction open porosity, $P = 0.15$, we predict the hardness of a zero porosity NBFO sample as $H_0 \sim 7.46$ GPa. Unfortunately there was no data available in the literature for comparison of the nanohardness and Young's modulus data measured and predicted in the present work. However, this data was comparable to the hardness data of 5–6 GPa reported for Ba-ferrites [28]. Nevertheless, this prediction would suggest that if a zero porosity NBFO sample can be made it will have a hardness most conducive to magnetoelectric memory device applications.

Annealing of the sample at a higher temperature would have caused agglomeration and increase in particle size. Therefore, an optimum low temperature of only 300 °C was deliberately chosen in the present work such as to totally avoid the particle growth and keep the sample effectively as good as a green NBFO pellet.

The aforesaid trend of experimentally measured data can also be explained in terms of an elastic recovery (ER) parameter. Physically, the ER parameter represents the ratio of elastically recovered depth $(h_m - h_f)$ to maximum depth (h_m) expressed as a percentage. Thus it gives an idea about what percentage of the maximum depth (h_m) was closed up as a result of the elastic recovery process. It is interesting to note that the ER parameter always decreased as the indentation load was increased (Fig. 6) i.e. the trend was similar to that of Fig. 5a which showed a decreasing trend of nanohardness with load. It means that at a lower load e.g. 100 μN the elastically recovered depth $(h_m - h_f)$ was a higher percentage of the maximum depth. This would imply a comparatively lower value of the final depth of penetration (h_f) suggesting that under such a situation a comparatively lower amount of energy was spent in causing permanent, plastic deformation in the NBFO sample. However, at a comparatively higher load e.g. 500 and or 1000 μN, the situation changes substantially. Here, the elastically recovered depth was a lower percentage of the maximum depth (Fig. 6). It implies a comparatively higher

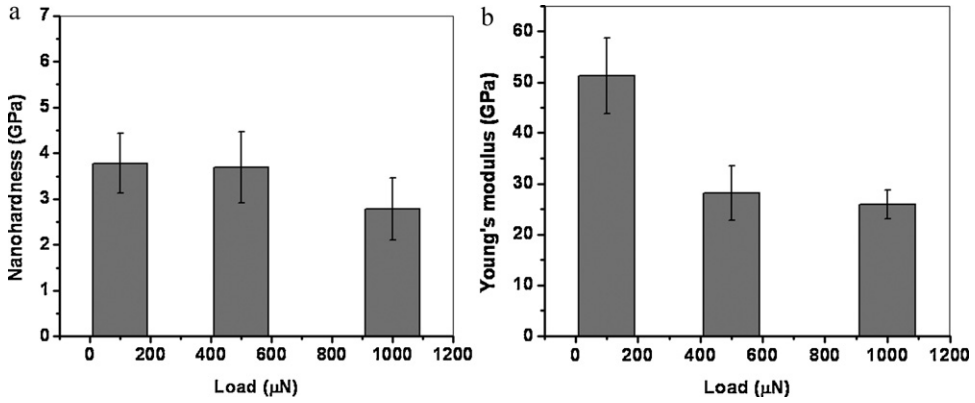

Fig. 5. Variation of data on (a) nanohardness and (b) Young's modulus for the green NBFO pellet as a function of indentation load.

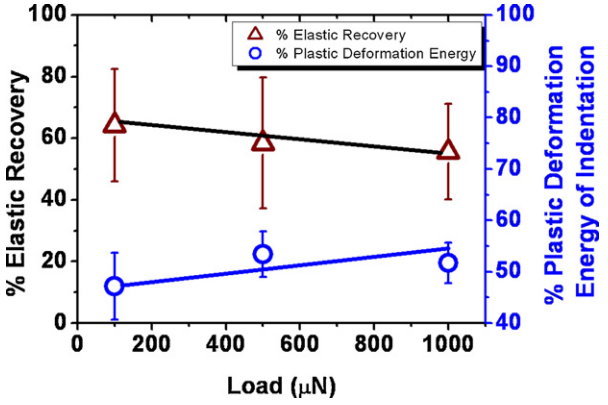

Fig. 6. Variation of ER parameter and the plastic deformation energy as a percentage of the total energy consumed during nanoindentation process of the green NBFO pellet as a function of indentation load.

value of the final depth of penetration. This data would suggest that under such a situation a comparatively higher amount of energy was spent in causing permanent, plastic deformation in the NBFO sample. If this picture is correct, then out of the total amount of energy spent in elastic and plastic deformation processes during the nanoindentation of the NBFO sample, the amount spent in causing permanent, plastic deformation of NBFO should increase with the nanoindentation load. A plot of the percentage of total energy of indentation spent in causing '*only plastic deformation*' as a function of load (Fig. 6) indeed corroborates this picture. It also follows then that the lower the final depth of penetration the smaller was the projected contact area and the hence the higher was the nanohardness measured at a lower load e.g. 100 μN. Similarly, the higher the final depth of penetration the larger was the projected contact area and the hence the lower was the nanohardness measured at a higher load e.g. 1000 μN, thereby giving rise to the indentation size effect as was observed (Fig. 5a) in the present experiments.

4. Conclusions

To the best of our knowledge the very first attempt was made in the present work to evaluate the nanomechanical properties of a nano $BiFeO_3$ sample. The nano $BiFeO_3$ (NBFO) powder was synthesized in the laboratory using a novel sol–gel route. The X-ray diffraction trace proved the presence of $BiFeO_3$ phase. The particle size of the NBFO powder was measured as 5–25 nm from the TEM study. The nanoindentation study was carried out at room temperature to measure the nanohardness and Young's modulus at three different loads e.g. 100, 500 and 1000 μN on the green NBFO pellet annealed at only 300 °C. The nanohardness value of the NBFO pellet was measured as ~3.8 GPa at 100 μN load which dropped to ~2.8 GPa at a rate of only 0.26 GPa μN^{-1} when the load was increased by an order of magnitude e.g. from 100 μN to 1000 μN. The corresponding Young's modulus values were ~51 GPa and ~26 GPa at 100 and 1000 μN loads, respectively. The decrease in hardness and Young's modulus were further explained with elastic recovery and plastic deformation energy concepts.

Acknowledgements

The authors (AKM and AD) thank Prof. I. Manna, Director, CGCRI for encouragements and CSIR (Project No: NWP 0027 and SRF ACK No.: 141011/2K8/2) for financial support.

References

[1] M.M. Kumar, V.R. Palkar, S.V. Suryanarayana, Ferroelectricity in a pure $BiFeO_3$ ceramic, Appl. Phys. Lett. 76 (2000) 2764–2766.
[2] J.V. Rivera, H. Scmid, On the birefringence of magnetoelectric $BiFeO_3$, Ferroelectrics 204 (1997) 23–33.
[3] D. Lebeugle, D. Colson, A. Forget, M. Viret, Very large spontaneous electric polarization in $BiFeO_3$ single crystals at room temperature and its evolution under cycling fields, Appl. Phys. Lett. 91 (2007) 022907.
[4] D. Lebeugle, D. Colson, A. Forget, M. Viret, P. Bonville, J.F. Marucco, S. Fusil, Room-temperature coexistence of large electric polarization and magnetic order in $BiFeO_3$ single crystals, Phys. Rev. B 76 (2007) 024116.
[5] W. Eerenstein, F.D. Morrison, J. Dho, M.G. Blamire, J.F. Scott, N.D. Mathur, Comment on 'epitaxial $BiFeO_3$ multiferroic thin film heterostructures', Science 307 (2005) 1203.
[6] J. Wang, J.B. Neaton, H. Zheng, V. Nagarajan, S.B. Ogale, B. Liu, D. Viehland, V. Vaithyanathan, D.G. Schlom, U.V. Waghmare, N.A. Spaldin, K.M. Rabe, M. Wuttig, R. Ramesh, Epitaxial $BiFeO_3$ multiferroic thin film heterostructures, Science 299 (2003) 1719–1722.
[7] T. Zhao, A. Scholl, F. Zavaliche, K. Lee, M. Barry, A. Doran, M.P.Y. Cruz, H. Chu, C. Ederer, N.A. Spaldin, R.R. Das, D.M. Kim, S.H. Baek, C.B. Eom, R. Ramesh, Electrical control of antiferromagnetic domains in multiferroic $BiFeO_3$ films at room temperature, Nat. Mater. 5 (2006) 823–829.
[8] J.R. Teague, R. Gerson, W.J. James, Dielectric hysteresis in single crystal $BiFeO_3$, Solid State Commun. 8 (1970) 1073–1074.
[9] A.V. Zalesskii, A.K. Zvezdin, A.A. Frolov, A.A. Bush, Fe-57 nmr study of a spatially modulated magnetic structure in $BiFeO_3$, JETP Lett. 71 (2000) 465–468.
[10] N. Orlovskaya, N. Browning, A. Nicholls, Ferroelasticity in mixed conducting $LaCoO_3$ based perovskites, Acta Mater. 51 (2003) 5063–5071.
[11] N. Orlovskaya, Y. Gogotsi, M. Reece, B. Cheng, I. Gibson, Ferroelasticity and hysteresis in $LaCoO_3$ based perovskites, Acta Mater. 50 (2002) 715–723.
[12] S.A.T. Redfern, C. Wang, J.W. Hong, G. Catalan, J.F. Scott, Elastic and electrical anomalies at low-temperature phase transitions in $BiFeO_3$, J. Phys.: Condens. Matter 20 (2008) 452205.
[13] C.W. Huang, L. Chen, J. Wang, Q. He, S.Y. Yang, Y.H. Chu, R. Ramesh, Phenomenological analysis of domain width in rhombohedral $BiFeO_3$ films, Phys. Rev. B 80 (2009) 140101.
[14] T. Leist, K.G. Webber, W. Jo, E. Aulbach, J. Rödel, A.D. Prewitt, J.L. Jones, J. Schmidlin, C.R. Hubbard, Stress induced structural changes in La-doped $BiFeO_3$–$PbTiO_3$ high temperature piezoceramics, Acta Mater. 58 (2010) 5962–5971.
[15] A. Bolshakov, G.M. Pharr, Influences of pileup on the measurement of mechanical properties by load and depth sensing indentation techniques, J. Mater. Res. 13 (1998) 1049–1058.
[16] W.C. Oliver, G.M. Pharr, An improved technique for determining hardness and elastic modulus using load and displacement sensing indentation experiments, J. Mater. Res. 7 (1992) 1564–1583.
[17] G. Feng, S. Qu, H. Huang, W.D. Nix, An analytical expression for the stress field around an elastoplastic indentation/contact, Acta Mater. 51 (2007) 2929–2938.
[18] J. Musil, F. Kune, H. Zeman, H. Polakova, Relationships between hardness, young's modulus and elastic recovery in hard nanocomposite coatings, Surf. Coat. Technol. 154 (2002) 304–313.
[19] M. Kanari, K. Tanaka, S. Baba, M. Eto, Nanoindentation behavior of a two-dimensional carbon–carbon composite for nuclear applications, Carbon 35 (1997) 1429–1437.
[20] W.D. Nix, H. Gao, Indentation size effects in crystalline materials: a law for strain gradient plasticity, J. Mech. Phys. Solid 46 (1998) 411–425.

[21] J.F. Li, S. Wang, K. Wakabayashi, M. Esashi, R. Watanabe, Properties of modified lead zirconate titanate ceramics prepared at low temperature (800 °C) by hot isostatic pressing, J. Am. Ceram. Soc. 83 (2000) 955–957.
[22] A.K. Mukhopadhyay, K.K. Phani, Young's modulus - porosity relations: an analysis based on a minimum contact area model, J. Mater. Sci. 33 (1998) 69–72.
[23] R.C. Rossi, Prediction of the elastic moduli of composites, J. Am. Ceram. Soc. 51 (1968) 433–439.
[24] A.K. Mukhopadhyay, S.K. Datta, D. Chakraborty, On the microhardness of silicon nitride and sialon ceramics, J. Eur. Ceram. Soc. 6 (1990) 303–311.
[25] A.K. Mukhopadhyay, S.K. Datta, D. Chakraborty, Hardness of silicon nitride and sialon, Ceram. Int. 17 (1991) 121–127.
[26] J. Luo, R. Stevens, Porosity-dependence of elastic moduli and hardness of 3Y-TZP ceramics, Ceram. Int. 25 (1999) 281–286.
[27] A. Dey, A.K. Mukhopadhyay, Anisotropy in nanohardness of micro-plasma sprayed hydroxyapatite coating, Adv. Appl. Ceram. 109 (2010) 346–354.
[28] Z. Li, G. Gao, Chemical bond and hardness of M-, W-type hexagonal barium ferrites, Can. J. Chem. 89 (2011) 573–576.